Establishment of a Rodent Model of Neural Injury After High Frequency Monopolar Stimulation of the Motor Cortex

Tao Yu
University of California, San Francisco
Lanjun Guo (lanjun.guo@ucsf.edu)
University of California, San Francisco
Jennifer Sasaki Russell
University of California, San Francisco
Jeffrey W. Sall
University of California, San Francisco

Research Article

Keywords: motor cortex, neural injury, rodent model, high-frequency stimulation (HFS)

Posted Date: February 10th, 2021

DOI: https://doi.org/10.21203/rs.3.rs-181181/v1

Abstract

Direct electrical motor cortex stimulation with short-train high-frequency stimulation (HFS) for motor evoked potentials (MEPs) has been used intraoperatively during supratentorial surgeries, but the safety threshold is poorly defined. The goal of this study is to establish a rat model for the investigation of neural damage in the cerebral cortex caused by high current HFS to aid in defining safety thresholds. We performed bilateral craniotomy on 12 rats. Cerebral sensory-motor cortex was stimulated with a high-frequency current for 100 times. The rats were sacrificed and the brains were sliced for Nissl, DAPI, and IBA-1 staining. Severe neural damage of the cerebral cortex was found in all cases, including markedly shrunken and pyknotic cells. IBA-1 staining revealed reactive microglia morphology in the lesion area. DAPI staining showed nucleus degeneration and deformation. The cell density were significantly lower within the lesion area compared to the contralateral side. This study has established a brain lesion model caused by HFS on rats. These results suggest HFS may carry a risk of serious neural damage if repeatedly applied to the same brain site. More experiments are needed to fully understand the safety threshold of direct cortical stimulation with HFS for clinical use.

Introduction

Intraoperative neurophysiological monitoring (IONM) has been used to reduce the risk of neurological deterioration during neurosurgical procedures[1–4]. In recent years, short-train high-frequency stimulation (HFS) has been widely used for functional mapping of the motor area and functional monitoring to detect motor dysfunction during intracranial surgery[5–12]. Direct application of electrical stimulation on the motor cortex may carry a risk of damage to the brain. Most previous studies that investigated safety parameters were based on continuously delivered current or prolonged, continuous 50-Hz biphasic rectangular pulse[13–17]. The safety thresholds for direct cortical stimulation with short-train HFS under varying parameters is largely unknown. At present, the current intensity is generally considered to be safe when under 30 mA[9,18]. However, pediatric patients often require higher current to trigger MEPs[19,20]. Under these circumstances, it is necessary to define the safe parameters of HFS to ensure that monitoring itself does not injure the patients.

The current safety thresholds used in the clinic for direct cortical stimulation with HFS for motor mapping and monitoring is based on continuously delivered current with low-frequency stimulation (LFS) since there are few studies based on HFS in human or animal models[13–17, 21,22]. A previous study reported that 50-mA current HFS caused mild and transient neural damage in the brain on transmission electron microscope slides[16]. No significant neural damage was observed under the light microscope. Thus, to develop a model a higher current HFS is required in order to induce significant neural injury. In this study, we used a protocol that goes beyond the typical needs of general clinical use. The primary goal of this study is to define characteristics of HFS-injury in the cerebral cortex in an animal model. This will facilitate further experiments to determine safe parameter combinations for HFS.

Results

Stimulation results

Each of the 12 rats received 100 times of short trains of HFS. All rats survived the duration of the experiment and respiration rates remained normal throughout stimulation. The motor evoked potential and muscle twitch were triggered during each stimulation. A summary of stimulation parameters is presented in Table 1.

Table 1
Electrical stimulation parameters in this study

Parameters	
Test number (n)	12
Type electrode	Platinum
Current (mA)	100
Frequency (Hz)	500
Pulse duration (msec)	0.5
Pulse number per train	5
Number of stimulation	100
ITI (second)	5 ~ 10
Total stimulation time (ms)	250
Stimulation Area (mm^2)	7.07
Current density (A/cm^2)	1.41
Q (μC)	50
Qt (μC)	25,000
QDt (C/cm^2)	0.35
QD ($\mu C/ cm^2$)	707
ITI, intertrial interval; Q, Charge per pulse; QD, Charge density; Qt, total charge; QDt, total charge density.	

Gross findings

After stimulation, the surface of focal dura mater just below and around the stimulated electrodes showed pink-brown color and swelling (Fig. 1B). The average diameter of the lesion on the brain's surface was 4.69 ± 0.56 mm, which was larger than the width of the electrode (3 mm). The surface of the brain was smooth and did not adhere to the dura. During the slicing, the cross section of the brain showed a light-brown colored cone-shaped lesion which had a relatively defined border (Fig. 1C).

Histological changes of the stimulation sites

The Nissl stained slices were examined under light-microscopy and revealed an edematous area extending through the cortex towards the subcortical corpus callosum and the lateral ventricle in a cone-shaped manner (Fig. 1D). There were 8 rats which presented with discrete hemorrhages within the brain parenchyma under the stimulation site (Fig. 1C). In the lesion area, there was increased extracellular space and shrunken cells in contrast to the normal tissue (Fig. 2A). All lesions showed severe damage and the neurons were markedly shrunken and dark in all grey layers and white matter. The columnar organization of neurons were disrupted in all layers. DAPI staining showed some nuclei were deformed (Fig. 3A-C). IBA-1 staining of microglia on the control side showed a ramified morphology. In contrast, most microglial under the stimulation site exhibited a dense, spherical morphology (Fig. 3D ~ F).

The average area of the lesion on the coronal section and the average volume of lesion with the largest lesion presentation are presented in Table 2. The average thickness of layer I, layer V, corpus callosum, and the entire cortex of the 12 rats were significantly larger on the stimulation side than the control side ($p < 0.001$, < 0.001, < 0.0001, < 0.0001, respectively) (Fig. 2B). The cell density of the lesion (2217.25 ± 248.59 particle/μm^2) was significantly lower than the control side (2544.21 ± 280.25 particle/μm^2) ($p < 0.001$) (Fig. 1E). The lateral ventricles and corpus callosum were compressed on the lesion side in all 12 cases. The average total cell area within the lesion was 36.77 ± 9.56 μm^2, which is significantly smaller than that of control side (117.93 ± 32.97 μm^2) ($p < 0.0001$) (Fig. 1E). In layer V, most of the motor cells appeared severely shrunken. The ratio of total cell area to total area was 6.42 ± 2.05 % in lesion and 27.41 ± 7.31 % in the corresponding part of the control side.

Table 2
Neural damage after stimulation of HFS

	Lesion side	Control side	*P*
Maximum lesion area (mm^2)	6.44 ± 1.33	n/a	
Maximum lesion deep (mm)	2.72 ± 0.31	n/a	
Lesion volume (mm^3)	16.16 ± 4.98	n/a	
Cell density (particle/mm^2)	2217.25 ± 248.59	2544.21 ± 280.25	< 0.001
Area of layer V cells to total area (%)	6.42 ± 2.05	27.41 ± 7.31	< 0.0001
Microglial damage (%)	100.0	no	
Discrete Hemorrhage (%)	66.7	no	
HFS, high frequency monopolar stimulation.			

Behavior assessment

No rats had visible major or minor seizure activity throughout the course of the study. None of the 12 rats showed abnormal EEG waves before or after stimulation. However, the EEG showed a very deep anesthesia pattern from the general anesthesia of isoflurane. All rats recovered well from anesthesia and exhibited no motor deficit or abnormal behavior within the 5 hours after stimulation and before sacrifice.

Discussion

In this experimental study, we established an animal model using rats that could simulate the potential brain damage from HFS. We delivered 100 trains of 100 mA HFS to the rat brain. After stimulation, the brains showed swelling and coloring consistent with hemorrhage or hemolysis on visual observation. Comparing Nissl, IBA-1 and DAPI staining from the electrode sites with comparable regions on the contralateral side, it was found that significant neural damage was associated with the electrical stimulation. These results indicate that the cortex may be injured by HFS if a certain safety threshold is exceeded.

The safety threshold for transcranial direct cortical stimulation is relatively well established, but has not been clearly identified for HFS[13,14,23]. In general, higher current intensity, total charge and total charge density will augment neuronal damage to brain tissue[24]. Oinuma et al. established an animal model and used 1.5 ~ 50 mA HFS repeated 100 times on rat sensorimotor cortex[16]. They didn't observe neural injury on light microscope. Janca et al. reported using a short sequence of 15 monophasic pulses of HFS up to 100 mA with 400 μs duration repeated 5 times on each site of the patients' brain, which did not cause

disruptive changes on histopathological examination[25]. However, the stimulating electrode for continuous MEP monitoring is usually placed at one spot with repeated stimulation during the whole surgical procedure.

Whenever current is used to stimulate brain, it may cause neural injury if the stimulus strength exceeds a certain level[21,25–31]. Both HFS and LFS were considered at risk for certain side effects, such as seizure, scalp burns, cardiac arrhythmia, tongue or lip laceration[3,13,15,32]. Although HFS is considered a relatively safe method, some patients, especially pediatric patients, require a higher current to trigger MEPs[19]. Standard electrical stimulation protocol is ineffective for 20% of young children[25]. Ng reported that in 10 of 15 cases with pediatric surgery, 50 to 90 volts were required for direct cortical stimulation to elicit MEPs[20]. Current intensity under 30 mA is usually considered safe in clinical use, but it is unclear what the safe stimulating threshold with higher electricity power is for HFS[3,30].

In order to establish a model, we used 100 mA HFS repeated 100 times to observe the potential neural damage. In our model, we didn't remove the thin dura mater because: (1) it is easy to injure the brain when removing it; and (2) the dura mater of the rat can reduce the gap of arachnoid membrane between rat and human brain[33]. In this study, the brain lesion included brain tissue edema, increased extracellular space, severely damaged neural cells, and hemorrhage, corresponding with lesions caused by electrical stimulation[21,26]. According to the grading of neuronal damage as described by Pudenz et al. and Yuen et al., all the rats had severe neural damage[21,26]. The DAPI staining also showed the severe injury of the cell nucleus[34]. IBA-1 staining revealed ramified or resting microglia on the control side. In the lesion, the microglia showed dense, spherical morphology which was consistent with reactive or phagocytic microglia. It is possible that severe neural damage induced microglial transformation into brain macrophages to remove dead cells within 5 hours of injury[35,36]. It was unclear whether the lesions can be completely repaired over time. If the lesion is severe and cannot be fully repaired, this process may result in glial scars.[37] It remains to be determined whether the damage we observed is transient or converts over time to a typical glial scar.

The charge density and charge per phase are neural excitotoxic cofactors[15,26]. Currently, the safety limits of the HFS technique applied in a short train over a longer period of time remains undefined. In this pilot study, the charge of one pulse was 50 μC, and the charge density was 707 $\mu C/cm^2$• pulse, which is very high compared to clinical standards. Severe neural damage was observed after 100 trains were delivered within 15 minutes. This finding demonstrates that repeated HFS at the same site may have a cumulative effect and is likely to cause severe neural damage.

Our study has established a rat model for studying neural damage caused by short-train HFS. The current parameters, while exceeding normal clinical standards, caused severe neural damage to the rat brain that are observable and quantifiable. Although it may be difficult to apply the safety limits from the animal histologic changes directly to humans, the neural damage observed may cause permanent neural damage in human brain that would increase the potential to induce seizure[38]. The primary effects appear

immediately as a direct result of the tissue or cellular injury, while the secondary effects may evolve over a longer period as a result of molecular signaling cascades that are activated by the initial injury. Longer observation post procedure may help define behavioral outcomes and whether the changes we observed are transient or persist and lead to scarring.

LIMITATIONS

The purpose of this study was to create an animal model of brain injury caused by direct cortical stimulation with HFS. Therefore, a relatively high current intensity, 100 mA, was used to stimulate. Future studies with varying levels of current intensity are necessary. The stimulating parameter in this study were based on the settings used for human patients with a larger brain volume and may not translate to the smaller rodent brain. The latency of MEPs recorded on rats was very short, so it was difficult to distinguish the MEP response from artifacts. Based on current study, we do not know the long-term effects of the morphological changes induced by the stimulation. Future studies will extend the survival time to observe the brain changes and animal behavior after a longer period and to determine stimulation parameters where damage is first observed.

Conclusions

This study has established a brain lesion model caused by direct cortical stimulation using HFS on rats. Gross observations, histological and immunohistochemistry methods, such as the Nissl, DAPI and IBA-1 staining were used to identify the injured cells and the phagocytic changes of microglia. Additional experiments are needed to fully define the safety threshold of direct cortical stimulation using short-train HFS, and the model established here can be easily replicated by different investigators attempting to study direct cortical HFS.

Methods

Animals

All studies were approved by the institutional animal care and use committee at University of California, San Francisco, and whenever possible the ARRIVE guidelines were followed. P23-P30 Sprague-Dawley male rats weighing 70–125 g were purchased from the Charles River Laboratories (Gilroy, CA, USA) and housed on a 12 h reverse light/dark cycle with *ad libitum* access to food and water.

Anesthesia and surgery protocol

Rats were anaesthetized in an induction chamber with 3.0% isoflurane, and then maintained with 1.0% of isoflurane in air and oxygen (FiO2 50%) for the surgery. Their heads were firmly fixed with ear bars in a stereotaxic frame (David Kopf Instruments, USA). A “U” shape incision was made to expose the skull.

Two craniotomies were performed, one on each hemisphere (3 mm above bregma and 5 mm below bregma with width of 5mm) using a drill. The dura mater was exposed for electrical stimulation (Fig. 1A).

Electrophysiological Stimulation protocol

A Cascade IOMAX (Cadwell Industries, Inc, USA) was used for stimulating and recording. The platinum electrode with 3 mm diameter of a Cortac® subdural strip electrode (PMT Corporation, USA) was fixed on the dura mater and used for stimulating. Digitized EEG was recorded during electrical stimulation and 15 minutes after from electrodes placed on the stimulated and contralateral sides. All 12 rats were randomly stimulated on one side of the sensory-motor cerebral cortex. The contralateral side was used as the control side. EMG responses were recorded from identical needle electrodes placed on the triceps brachii and triceps surae muscle. After the stimulation protocol was completed, the skin was closed with suture. All rats were awakened and survived for 5 hours, then were sacrificed for further analysis.

Parameters of electrical stimulation

The stimulus intensity was 100 mA. Complete parameters are listed in Table 1. Charge per pulse(Q) is defined as I (current intensity) × D (duration of each pulse) for the rectangular pulses. Charge density (QD) (in microcoulumbs/cm^2, or μC/cm^2) is charge divided by electrode area. Total charge (Qt) and total charge density (QDt) are defined as Q or QD times the number of pulses.[23] Current density (in A/cm^2) is applied current at the electrode divided by electrode area.

Brain tissue processing and immunohistochemistry

The rats were anesthetized again with isoflurane and perfused with 0.01 mol/L phosphate-buffered saline (PBS) (30 mL) and 4% paraformaldehyde (PFA) solution (150 mL). After decapitation, the skulls were opened and brains were carefully dissected. The brains were stored in PFA overnight, then transferred into 30% sucrose. Then they were rapidly frozen and stored in isopentane at -20 °C. 40 μm thick coronal sections were cut on a Leica CM 1850 cryostat (Leica Microsystems, GmbH, Nussloch, Germany) and mounted onto glass slides. The slides were stained by the Nissl method with cresyl violet and used for quantitative analyses.

Free floating sections in the PBS were incubated for 1 hour with 1:2,500 rabbit-anti IBA-1 (Abcam Inc, Toronto, ON, Canada, C), 1 hour with 1:500 Alexa Fluor 594 goat anti-rabbit secondary antibody (Molecular probes, Eugene, OR, USA), 5 min with 1:5,000 DAPI (Vector Laboratories) at room temperature. Sections were mounted onto glass slides and sealed with Fluoro-Gel mounting media and cover slipped.

The slices were scanned by Cytation 5 imaging reader (4X and 20X) (BioTek instruments, inc., USA). Image processing, measurements and cell counts were performed using the FIJI software.[39] The area and volume of each lesion were calculated by its diameter and deepness. Cell counts were obtained by setting the intensity threshold then running the particle count analysis. The cell density was calculated by cell counts divided by area, and the lesion side was contrasted with the control side. The proportion of cell

area was calculated by total cell area divided by total area. The thickness of cell layers of cerebral cortex was measured using FIJI software.

Statistical Analysis

Statistical processing and analysis of results were conducted using SPSS (IBM corp., Chicago, USA). The significance of differences was assessed using the two tailed t test for independent variables. *P* values less than 0.05 were considered statistically significant. All data were expressed as the mean ± standard deviation.

Declarations

Author contributions

T.Y., L.G. performed the animal surgery and HFS stimulation. T.Y. performed the staining of the study, analysed results and prepared the manuscript. T.Y., L.G. and J.S. interpreted and integrated all the data. T.Y., L.G. and J.R. wrote the manuscript with input from all coauthors. All authors approved the final version of the manuscript. L.G., J.R and J.S. supervised the research.

Competing interests

The author(s) declare no competing interests.

References

1. Berger, M. S., Cohen, W. A. & Ojemann, G. A. Correlation of motor cortex brain mapping data with magnetic resonance imaging. *Journal of neurosurgery* **72**, 383-387, doi:10.3171/jns.1990.72.3.0383 (1990).
2. Taniguchi, M., Cedzich, C. & Schramm, J. Modification of cortical stimulation for motor evoked potentials under general anesthesia: technical description. *Neurosurgery* **32**, 219-226, doi:10.1227/00006123-199302000-00011 (1993).
3. Sartorius, C. J. & Wright, G. Intraoperative brain mapping in a community setting--technical considerations. *Surg Neurol* **47**, 380-388, doi:10.1016/s0090-3019(96)00340-0 (1997).
4. Krombach, G. A., Spetzger, U., Rohde, V. & Gilsbach, J. M. Intraoperative localization of functional regions in the sensorimotor cortex by neuronavigation and cortical mapping. *Comput Aided Surg* **3**, 64-73, doi:10.1002/(SICI)1097-0150(1998)3:2<64::AID-IGS3>3.0.CO;2-I (1998).
5. Cedzich, C., Taniguchi, M., Schafer, S. & Schramm, J. Somatosensory evoked potential phase reversal and direct motor cortex stimulation during surgery in and around the central region. *Neurosurgery* **38**, 962-970, doi:10.1097/00006123-199605000-00023 (1996).
6. Kombos, T., Suess, O., Funk, T., Kern, B. C. & Brock, M. Intra-operative mapping of the motor cortex during surgery in and around the motor cortex. *Acta Neurochir (Wien)* **142**, 263-268, doi:10.1007/s007010050034 (2000).

7. Horiuchi, K. *et al.* Intraoperative monitoring of blood flow insufficiency during surgery of middle cerebral artery aneurysms. *Journal of neurosurgery* **103**, 275-283, doi:10.3171/jns.2005.103.2.0275 (2005).
8. Kawaguchi, M. *et al.* Intraoperative myogenic motor evoked potentials induced by direct electrical stimulation of the exposed motor cortex under isoflurane and sevoflurane. *Anesth Analg* **82**, 593-599, doi:10.1097/00000539-199603000-00029 (1996).
9. Kombos, T., Suess, O., Ciklatekerlio, O. & Brock, M. Monitoring of intraoperative motor evoked potentials to increase the safety of surgery in and around the motor cortex. *Journal of neurosurgery* **95**, 608-614, doi:10.3171/jns.2001.95.4.0608 (2001).
10. Neuloh, G., Pechstein, U., Cedzich, C. & Schramm, J. Motor evoked potential monitoring with supratentorial surgery. *Neurosurgery* **54**, 1061-1070; discussion 1070-1062, doi:10.1227/01.neu.0000119326.15032.00 (2004).
11. Sakuma, J. *et al.* Monitoring and preventing blood flow insufficiency due to clip rotation after the treatment of internal carotid artery aneurysms. *Journal of neurosurgery* **100**, 960-962, doi:10.3171/jns.2004.100.5.0960 (2004).
12. Szelenyi, A. *et al.* Motor evoked potential monitoring during cerebral aneurysm surgery: technical aspects and comparison of transcranial and direct cortical stimulation. *Neurosurgery* **57**, 331-338; discussion 331-338, doi:10.1227/01.neu.0000176643.69108.fc (2005).
13. Bikson, M. *et al.* Safety of Transcranial Direct Current Stimulation: Evidence Based Update 2016. *Brain Stimul* **9**, 641-661, doi:10.1016/j.brs.2016.06.004 (2016).
14. Calancie, B., Harris, W., Broton, J. G., Alexeeva, N. & Green, B. A. "Threshold-level" multipulse transcranial electrical stimulation of motor cortex for intraoperative monitoring of spinal motor tracts: description of method and comparison to somatosensory evoked potential monitoring. *Journal of neurosurgery* **88**, 457-470, doi:10.3171/jns.1998.88.3.0457 (1998).
15. McCreery, D. B., Agnew, W. F., Yuen, T. G. & Bullara, L. Charge density and charge per phase as cofactors in neural injury induced by electrical stimulation. *IEEE Trans Biomed Eng* **37**, 996-1001, doi:10.1109/10.102812 (1990).
16. Oinuma, M. *et al.* High-frequency monopolar electrical stimulation of the rat cerebral cortex. *Neurosurgery* **60**, 189-196; discussion 196-187, doi:10.1227/01.NEU.0000249204.81472.88 (2007).
17. McCreery, D. B., Agnew, W. F., Yuen, T. G. & Bullara, L. A. Comparison of neural damage induced by electrical stimulation with faradaic and capacitor electrodes. *Ann Biomed Eng* **16**, 463-481, doi:10.1007/bf02368010 (1988).
18. Cedzich, C., Pechstein, U., Schramm, J. & Schafer, S. Electrophysiological considerations regarding electrical stimulation of motor cortex and brain stem in humans. *Neurosurgery* **42**, 527-532, doi:10.1097/00006123-199803000-00018 (1998).
19. Yi, Y. G. *et al.* Feasibility of intraoperative monitoring of motor evoked potentials obtained through transcranial electrical stimulation in infants younger than 3 months. *Journal of neurosurgery. Pediatrics*, 1-9, doi:10.3171/2019.1.PEDS18674 (2019).

20. Ng, W. H. *et al.* Stimulation threshold potentials of intraoperative cortical motor mapping using monopolar trains of five in pediatric epilepsy surgery. *Childs Nerv Syst* **26**, 675-679, doi:10.1007/s00381-009-0996-2 (2010).
21. Pudenz, R. H., Agnew, W. F. & Bullara, L. A. Effects of electrical stimulation of brain. *Brain Behav Evol* **14**, 103-125, doi:10.1159/000125578 (1977).
22. Vrba, J. *et al.* Modeling of Brain Tissue Heating Caused by Direct Cortical Stimulation for Assessing the Risk of Thermal Damage. *IEEE Trans Neural Syst Rehabil Eng* **27**, 440-449, doi:10.1109/TNSRE.2019.2898253 (2019).
23. MacDonald, D. B. Safety of intraoperative transcranial electrical stimulation motor evoked potential monitoring. *J Clin Neurophysiol* **19**, 416-429, doi:10.1097/00004691-200210000-00005 (2002).
24. Liebetanz, D. *et al.* Safety limits of cathodal transcranial direct current stimulation in rats. *Clin Neurophysiol* **120**, 1161-1167, doi:10.1016/j.clinph.2009.01.022 (2009).
25. Janca, R. *et al.* Intraoperative Thermography of the Electrical Stimulation Mapping: A Safety Control Study. *IEEE Trans Neural Syst Rehabil Eng* **26**, 2126-2133, doi:10.1109/TNSRE.2018.2871875 (2018).
26. Yuen, T. G., Agnew, W. F., Bullara, L. A., Jacques, S. & McCreery, D. B. Histological evaluation of neural damage from electrical stimulation: considerations for the selection of parameters for clinical application. *Neurosurgery* **9**, 292-299 (1981).
27. Gordon, B. *et al.* Parameters for direct cortical electrical stimulation in the human: histopathologic confirmation. *Electroencephalogr Clin Neurophysiol* **75**, 371-377, doi:10.1016/0013-4694(90)90082-u (1990).
28. Levi, H. *et al.* Stimulation of the sphenopalatine ganglion induces reperfusion and blood-brain barrier protection in the photothrombotic stroke model. *PLoS One* **7**, e39636, doi:10.1371/journal.pone.0039636 (2012).
29. Liu, H. *et al.* The Clinical and Medicolegal Analysis of Electrical Shocked Rats: Based on the Serological and Histological Methods. *BioMed research international* **2016**, 4896319, doi:10.1155/2016/4896319 (2016).
30. Yoshida, G. *et al.* Adverse Events Related to Transcranial Electric Stimulation for Motor-evoked Potential Monitoring in High-risk Spinal Surgery. *Spine (Phila Pa 1976)* **44**, 1435-1440, doi:10.1097/BRS.0000000000003115 (2019).
31. Kawaguchi, M. *et al.* Intraoperative electrophysiologic monitoring of ocular motor nerves under conditions of partial neuromuscular blockade during skull base surgery. *Skull Base Surg* **6**, 9-15, doi:10.1055/s-2008-1058908 (1996).
32. Szelenyi, A., Joksimovic, B. & Seifert, V. Intraoperative risk of seizures associated with transient direct cortical stimulation in patients with symptomatic epilepsy. *J Clin Neurophysiol* **24**, 39-43, doi:10.1097/01.wnp.0000237073.70314.f7 (2007).
33. Costa Ade, M. *et al.* An experimental model for the study of craniofacial deformities. *Acta Cir Bras* **25**, 264-268, doi:10.1590/s0102-86502010000300008 (2010).

34. Limoa, E. *et al.* Electroconvulsive shock attenuated microgliosis and astrogliosis in the hippocampus and ameliorated schizophrenia-like behavior of Gunn rat. *J Neuroinflammation* **13**, 230, doi:10.1186/s12974-016-0688-2 (2016).
35. Streit, W. J., Walter, S. A. & Pennell, N. A. Reactive microgliosis. *Prog Neurobiol* **57**, 563-581, doi:10.1016/s0301-0082(98)00069-0 (1999).
36. Davis, E. J., Foster, T. D. & Thomas, W. E. Cellular forms and functions of brain microglia. *Brain Res Bull* **34**, 73-78, doi:10.1016/0361-9230(94)90189-9 (1994).
37. Fawcett, J. W. & Asher, R. A. The glial scar and central nervous system repair. *Brain Res Bull* **49**, 377-391, doi:10.1016/s0361-9230(99)00072-6 (1999).
38. Mountney, A. *et al.* Functional and Molecular Correlates after Single and Repeated Rat Closed-Head Concussion: Indices of Vulnerability after Brain Injury. *J Neurotrauma* **34**, 2768-2789, doi:10.1089/neu.2016.4679 (2017).
39. Schindelin, J. *et al.* Fiji: an open-source platform for biological-image analysis. *Nat Methods* **9**, 676-682, doi:10.1038/nmeth.2019 (2012).

Figures

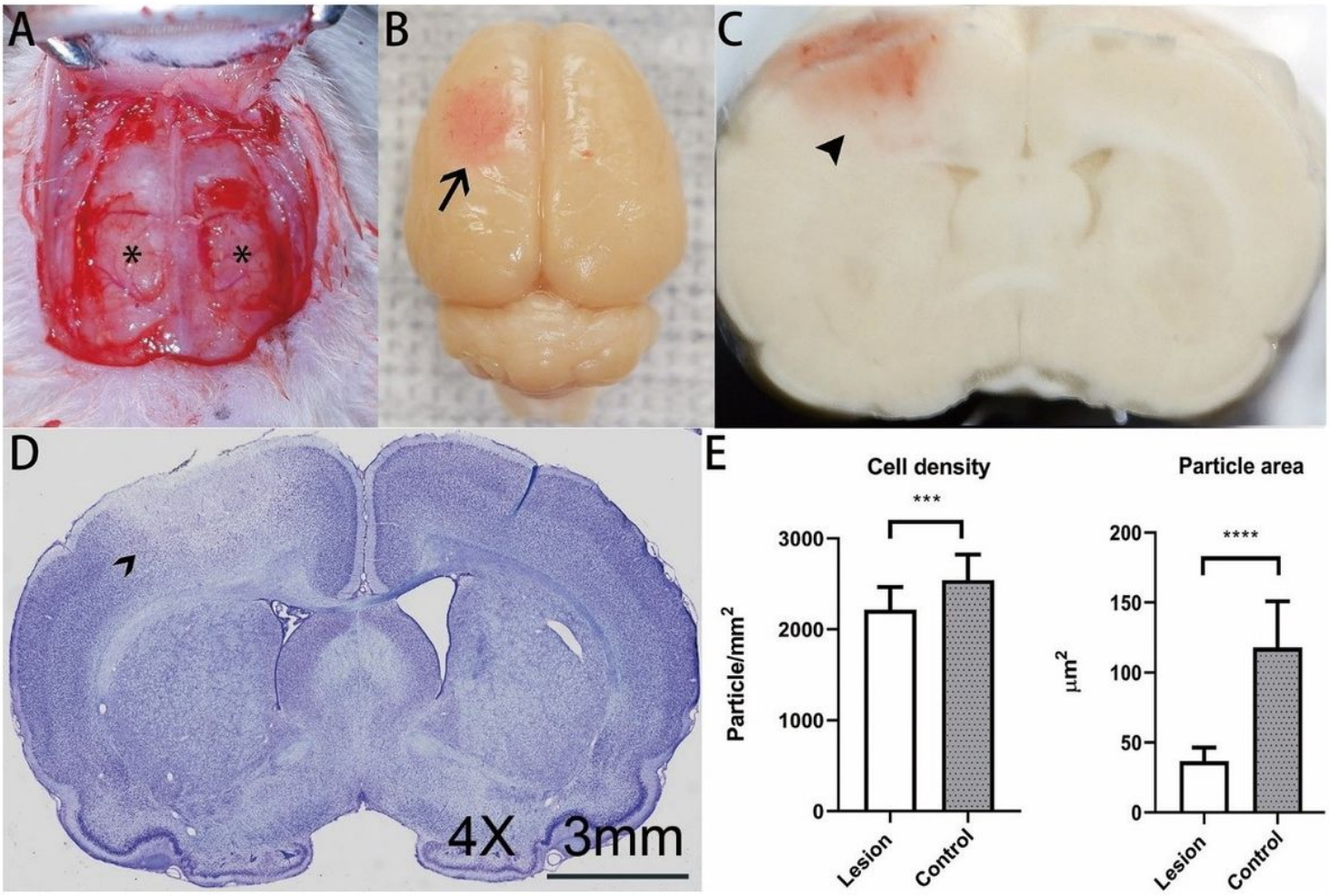

Figure 1

Bilateral side craniotomy of rat (A), and the dura mater was exposed (*). After stimulation and perfusion, the brain was dissected. The lesion beneath the stimulation site on the brain surface was pink (B) (arrow). The coronal section showed the lesion was a pink color cone-shaped lesion (arrow head) which had a relatively defined border (C). Light microscopy of the section also showed an edematous area in a conical manner (arrow head) (D) (Nissl stain, 4X). The cell density and average cell size were significantly lower in the lesion than the control side (E). Solid bar represents mean value. Error bars represent standard deviation. *** p 0.001, *** p < 0.0001.

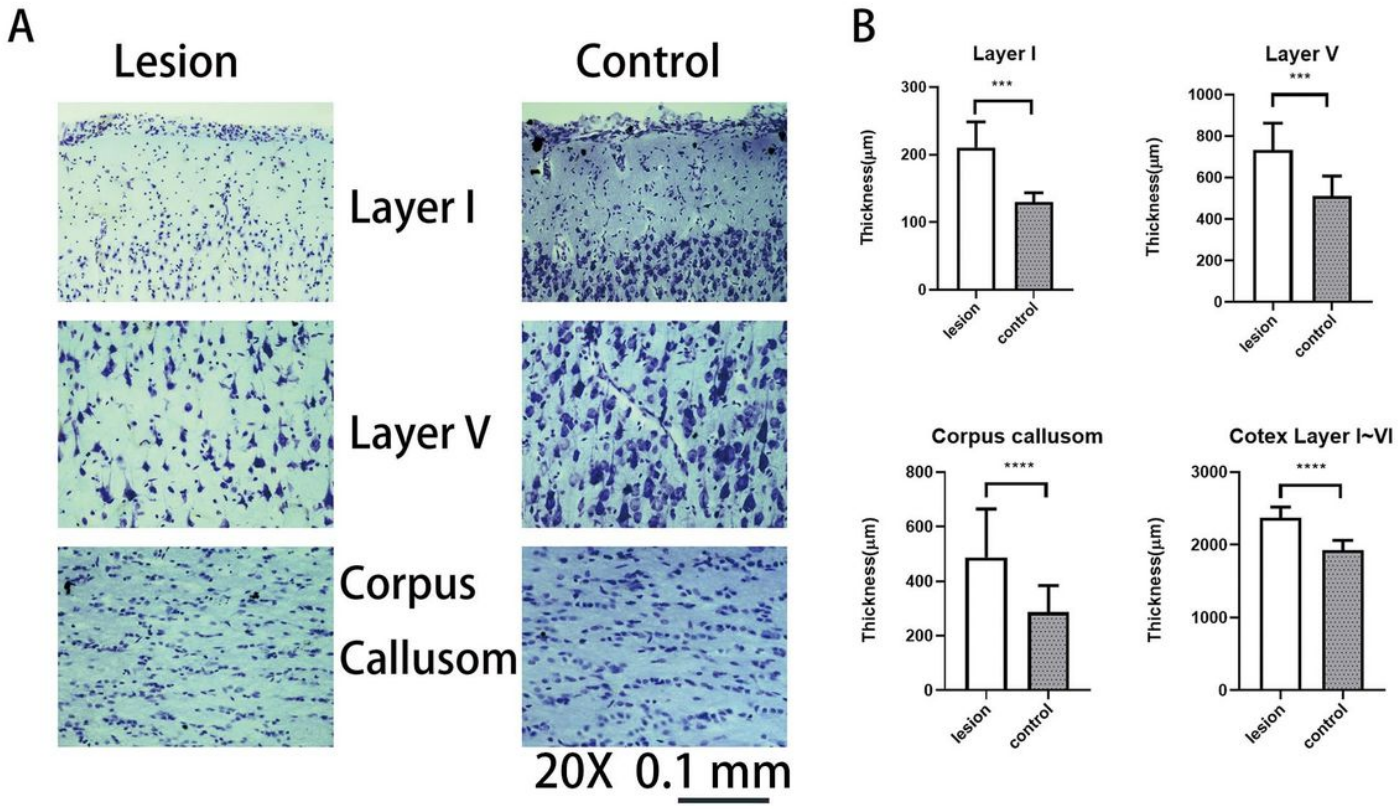

Figure 2

Light microscopy of layer I, layer V, and corpus callosum showed severe neural damage, and the neurons were markedly shrunken and dark (A) (Nissl stain, 20X). The thickness of layer I, layer V, corpus callosum, and the gray matter (layer I ~ layer V) were significantly larger than the control side (B). Solid bar represents mean value. Error bars represent standard deviation. *** p 0.001, *** p < 0.0001.

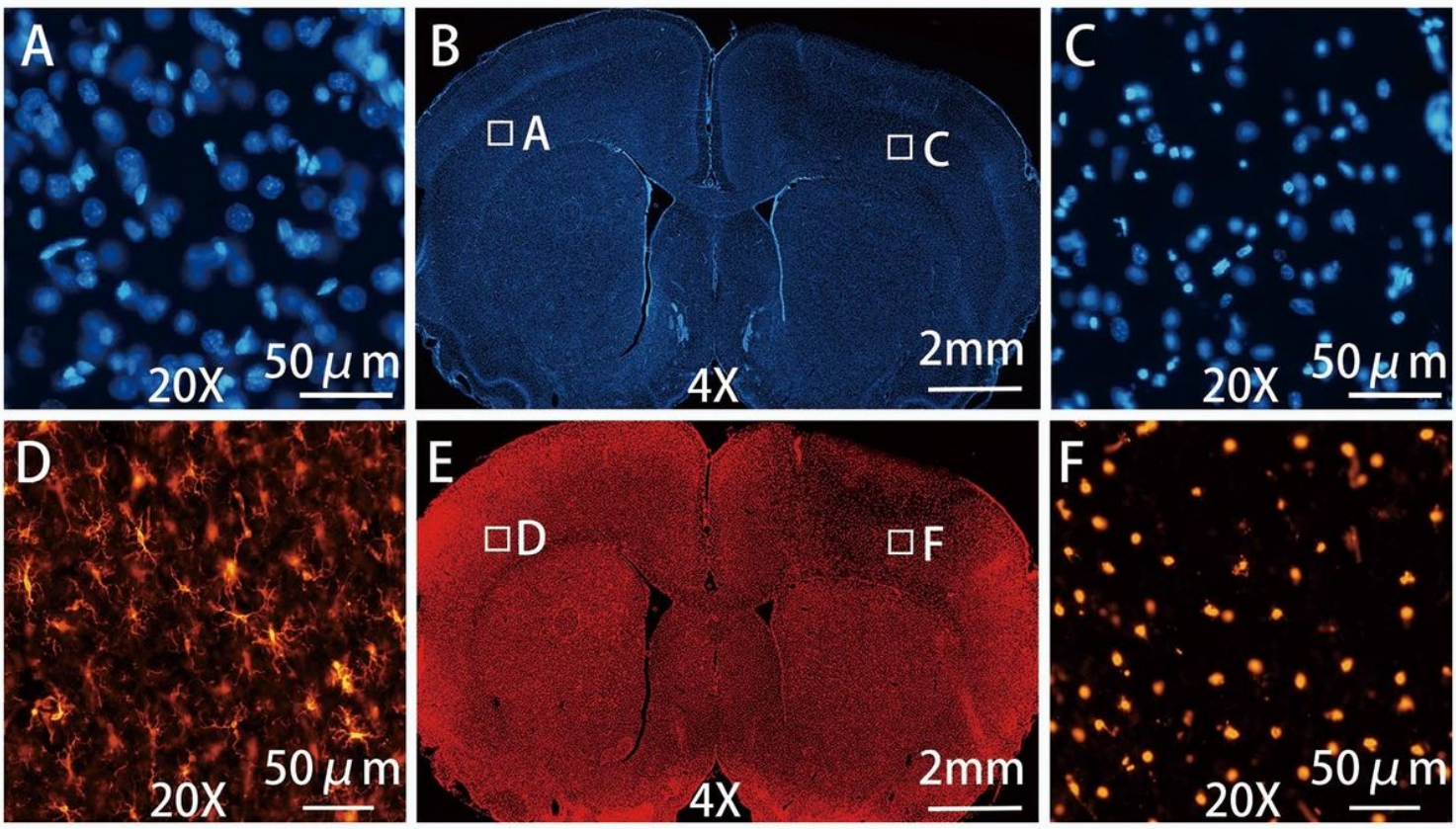

Figure 3

The DAPI staining (B) showed normal cell nucleus of the control side (A) (20X) and the loosened and deformed nucleus in the lesion (C) (20X). The IBA-1 staining (E) showed ramified (or resting) microglia on the control side (D) (20X) and reactive (or phagocytic) microglia in the lesion (F) (20X).